

RESEARCH ARTICLE

Novel magnetometer-free inertial-measurement-unit-based orientation estimation approach for measuring upper limb kinematics

Souha Baklouti^{1,2} , Taysir Rezgui³, Abdelbadia Chaker^{1,4}, Anis Sahbani^{2,5} and Sami Bennour^{1,6,7}

¹Mechanical Laboratory of Sousse (LMS), National School of Engineers of Sousse, University of Sousse, Sousse, Tunisia

²ENOVA Robotics S.A., Sousse, Tunisia

³Applied Mechanics, and Systems Research Laboratory (LASMAR), Tunisia Polytechnic School, University of Carthage, La Marsa, Tunisia

⁴Department of GMSC, Pprime Institute CNRS, ENSMA, UPR 3346, University of Poitiers, Poitiers, France

⁵Sorbonne University, Paris, France

⁶National School of Engineers of Monastir, University of Monastir, Monastir, Tunisia

⁷Computer Engineering, Production and Maintenance Laboratory (LGIPM), University of Lorraine, Metz, France

Corresponding author: Souha Baklouti; Email: baklouti.souha@eniso.u-sousse.tn

Received: 21 August 2024; **Revised:** 25 March 2025; **Accepted:** 23 April 2025

Keywords: inertial measurement units; sensor fusion; magnetometer-free orientation estimation; upper limb kinematics

Abstract

This study addresses challenges in sensor fusion for accurate and robust joint orientation estimation in human movement analysis using wearable inertial measurement units (IMUs). A magnetometer-free refined Kalman filter (KF) approach is presented and validated to address various indoor environmental constraints and challenges posed by human movement. These include variability in motion and dynamics, as well as magnetic disturbances caused by ferromagnetic materials or electronic interferences. Our proposed approach utilizes a Kalman-filter-based framework that analyzes the accelerometer's alignment with the Earth's frame to estimate orientation and correct gyroscope readings, eliminating reliance on magnetometer inputs. The algorithm was tested on both controlled robotic movements and real-world upper-limb-motion-monitoring scenarios. First, a comparative analysis was conducted on the double-stage Kalman filter (DSKF) and complementary filter using the collected robot motion encoder data. The results demonstrated superior performance in orientation estimation, particularly in yaw measurements, where the proposed method significantly improved accuracy. It achieved a lower root mean square error (RMSE = 2.447°) and mean absolute error (MAE = 2.006°), outperforming both the DSKF and complementary filter approaches. Additionally, the study's findings were validated against a standard motion capture system, revealing error metrics within generally acceptable ranges ($\leq 12.4\%$ of the joint range of motion [ROM]) and strong correlation coefficients ($r^2 > 0.89$). However, some deviations were observed during complex motion cycle intervals, highlighting opportunities for further refinement. These findings suggest that the proposed approach presents a promising alternative for human joint orientation estimation in industrial settings with magnetic distortions.

1. Introduction

Inertial measurement units (IMUs) have gained significant interest in recent years as a wearable tool for quantifying human movement. These systems are wireless, wearable, noninvasive and can provide real-

time data, making them a potential alternative to traditional motion capture methods such as optical systems. This technique is particularly used for monitoring the kinematics of the body's articulated structures composed of rigid segments (limbs or body parts) connected by joints (articulations). In such applications, one IMU per segment is used for several applications, such as biomechanics, ergonomics, and sports (Baklouti et al., 2024; Fain et al., 2024; Vigne et al., 2020). This approach also comes with several challenges, such as the random nature of movements due to high number of degrees of freedom and variable dynamics, which eliminate the possibility of relying on movement patterns to improve motion estimation.

The fusion of gyroscope, accelerometer, and magnetometer data enables the estimation of joint angles in articulated structures. Data from the magnetometer help to identify the system's orientation relative to the Earth's magnetic north, necessitating adequate calibration. Thus, the reliability of joint angle estimation becomes dependent on the magnetometer data and adequate calibration procedures, which limit system versatility. Indoor environments containing ferromagnetic materials and electronic devices can distort the local magnetic field, leading to orientation errors (Fan et al., 2017; Laidig and Seel, 2023).

Such magnetic disturbances compromise the accuracy and reliability of orientation data, making magnetometer-dependent systems less robust in real-world conditions (Rogers et al., 2011). Furthermore, magnetometer calibration is a complex and time-consuming process that often requires specialized equipment and procedures. Even after calibration, magnetometer performance remains highly sensitive to prolonged use and variations in the surrounding magnetic environment (Yadav and Bleakley, 2014). This further highlights the need for methods that can provide consistent and accurate orientation estimates without relying on the magnetic field.

To address these challenges, current research has explored sensor fusion techniques that exclude magnetometers. These approaches often employ advanced algorithms to integrate data from multiple gyroscope and accelerometer sensors and estimate orientation accurately. Madgwick et al. (2011) developed a gradient descent algorithm that uses accelerometer data to correct gyroscope measurements. This is achieved by iteratively minimizing the error between estimated and measured accelerations to refine orientation estimates. In addition, Kim and Golnaraghi (2004) present a quaternion-based KF for orientation estimation using only gyroscope and accelerometer data. Their method avoids the use of magnetometers by relying on the relationship between the quaternion representing the platform orientation and the measurements of gravity from the accelerometers, combined with angular rate measurements from the gyros. This approach demonstrated accurate and stable orientation estimates over long periods without the need for magnetometers (Kim and Golnaraghi, 2004). Similarly, the versatile quaternion-based filter (VQF) algorithm proposed by Laidig and Seel (2023) utilizes a quaternion-based orientation estimation algorithm that integrates gyroscope and accelerometer data. This approach includes a novel filtering technique for acceleration measurements and incorporates gyroscope bias estimation to enhance accuracy, outperforming eight other literature methods (Laidig and Seel, 2023).

Despite these advancements, several critical gaps in orientation estimation methods remain unaddressed. The gradient descent method proposed by Madgwick et al., 2011, for example, relies on initial assumptions that may not hold across various environments. Similarly, the method by Kim and Golnaraghi (2004) is based on the premise of stable and predictable motion patterns, which are often not present in dynamic or complex environments, such as human motion analysis. This can lead to significant errors, resulting in unreliable orientation estimates under challenging conditions (Bernal-Polo and Martínez Barberá, 2017). Additionally, the VQF algorithm, noted for its high accuracy (Laidig and Seel, 2023), requires meticulous parameter tuning and considerable computational resources. This may hinder its deployment in real-time applications on devices with limited processing power. This algorithm also assumes specific characteristics of magnetic disturbances and motion dynamics, potentially limiting its effectiveness in diverse real-world scenarios. Furthermore, Zihajehzadeh and Park (2017) have highlighted the challenges faced by various magnetometer-free filters, particularly in maintaining long-term stability and accurate yaw estimation. These filters struggle to completely eliminate drift without magnetometer data, impacting their effectiveness. While accelerometers perform well in correcting roll and pitch orientations (Łuczak et al., 2022), they face difficulties with yaw angle corrections (Kim and

Golnaraghi, 2004). Traditional yaw measurements utilize magnetometers to detect the Earth's magnetic field direction (Xiaoping et al., 2008); however, accelerometers, which measure linear acceleration and gravitational forces, do not directly inform about the heading relative to the magnetic field (Halitim et al., 2023), further complicating accurate orientation estimation using accelerometer data alone.

This study addresses these identified research gaps by developing sensor fusion algorithms adapted to varying environments for human body joint angle estimation with minimal manual calibration. The focus is on an adaptive orientation estimation method that functions effectively across diverse motion directions and dynamics without requiring extensive calibration processes. Moreover, the approach is designed to be robust in environments with fluctuating magnetic fields, ensuring reliable performance even in the presence of magnetic disturbances.

Specifically, the research introduces a novel magnetometer-free approach that uses the Kalman filter to enhance orientation estimation by analyzing the accelerometer's alignment with the Earth's frame. This method's accuracy is assessed against well-known algorithms, such as complementary filters and a DSKF, and benchmarked against a reference sensor solution. Additionally, the study evaluates the practical application of this method in upper limb motion monitoring. Comparisons are made with a standard motion capture system to test the method's integration and effectiveness in real-world scenarios. Through statistical analysis, the study seeks to identify differences between the systems and determine the factors that impact the accuracy of IMU-based measurements, thereby offering potential improvements in sensor fusion technology for dynamic and complex environments.

2. Methods

2.1. Proposed magnetometer-free orientation estimation approach design

The primary objective of the proposed algorithm is to estimate the orientation of wearable IMUs in environments prone to magnetic interference. Figure 1 showcases a simplified block diagram of the proposed orientation estimation algorithm.

The inputs for the algorithm include:

- Gyroscope measurements ω , representing angular velocity readings along the three axes (X, Y, Z).
- Accelerometer measurements \mathbf{a} , providing acceleration readings along the three axes (X, Y, Z).
- The time step dt , representing the sampling interval between consecutive measurements.
- The output of the algorithm is the state vector \mathbf{x} (Equation 2.1). It includes:

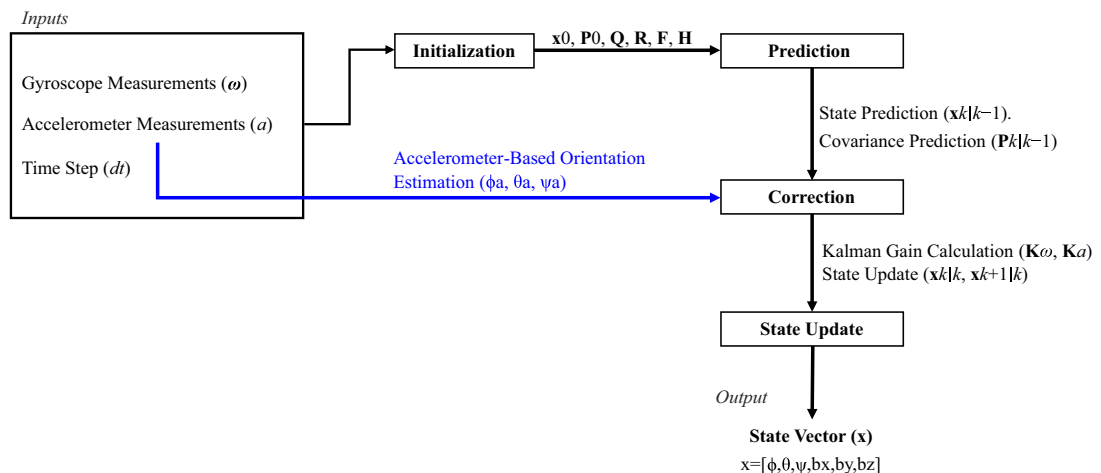


Figure 1. Simplified block diagram of the proposed orientation estimation algorithm for wearable IMUs.

- Orientation angles (roll ϕ , pitch θ , yaw ψ) relative to the Earth’s frame.
- Corrected gyroscope biases (b_x, b_y, b_z) along the three axes (X, Y, Z), accounting for errors in gyroscope readings.

$$\mathbf{x} = [\phi, \theta, \psi, b_x, b_y, b_z]^T. \tag{2.1}$$

The proposed algorithm utilizes a refined Kalman filter (KF) framework to fuse sensor data in three iterative steps: initialization, prediction, and correction. These steps estimate the orientation angles and correct gyroscope drift.

The algorithm begins by setting the initial values of the parameters, which are empirically tuned based on sensor noise statistics and system requirements:

- An initial 6×1 state vector (\mathbf{x}_0) that represents the system’s initial orientation (roll ϕ , pitch θ , yaw ψ) and gyroscope biases (b_x, b_y, b_z). Initially, all elements of this vector are set to zero, assuming no prior knowledge of the orientation or biases.
- An initial 6×6 symmetric state covariance matrix (\mathbf{P}_0) that captures the uncertainty in the state estimates. Each entry quantifies the variance or covariance of state variables, derived from the standard deviations (stds) of roll, pitch, yaw, and gyroscope biases. This matrix is initialized based on the expected noise characteristics of the sensors.
- A 6×6 process noise covariance matrix (\mathbf{Q}) that models uncertainty in the state prediction due to sensor noise characteristics.
- A 3×3 diagonal measurement noise covariance matrix (\mathbf{R}) that characterizes sensor noise during the correction step.
- A 6×6 state transition matrix (\mathbf{F}) that models the evolution of the state over time. It incorporates angular velocity integration and gyroscope bias dynamics, with the parameter dt representing the sampling interval between measurements.
- A 3×6 measurement matrix (\mathbf{H}) that maps the state vector to the estimated tilt angles. It extracts the relevant components of the state vector (roll, pitch, and yaw) for comparison with sensor data.

In the prediction step, the state \mathbf{x} and covariance \mathbf{P} are projected forward using the state transition matrix \mathbf{F} and process noise covariance \mathbf{Q} , as described in Equations (2.2) and (2.3):

$$\mathbf{x}_{k|k-1} = \mathbf{F} \cdot \mathbf{x}_{k-1}, \tag{2.2}$$

$$\mathbf{P}_{k|k-1} = \mathbf{F} \cdot \mathbf{P}_{k-1} \cdot \mathbf{F}^T + \mathbf{Q}. \tag{2.3}$$

The proposed method determines orientations from accelerometer data by aligning the sensor frame with the global Cartesian frame (Earth’s frame), enabling the correction of gyroscope drift. When static, accelerometer readings reflect the projection of gravity (\mathbf{g}) along its axes. A rotation matrix $\mathbf{R}_{\text{align}}$ aligns the sensor frame with the global frame, as given in Equations (2.4) and (2.5):

$$\tilde{\omega}_{\text{ref}} = \mathbf{R}_{\text{align}}^T \cdot \tilde{\omega}, \tag{2.4}$$

$$\tilde{\mathbf{a}}_{\text{ref}} = \mathbf{R}_{\text{align}}^T \cdot \tilde{\mathbf{a}}. \tag{2.5}$$

Here, $\tilde{\omega}_{\text{ref}}$ and $\tilde{\mathbf{a}}_{\text{ref}}$ represent angular velocity and acceleration in the Earth’s reference frame, respectively, while $\tilde{\omega}$ and $\tilde{\mathbf{a}}$ represent their respective values in the sensor frame.

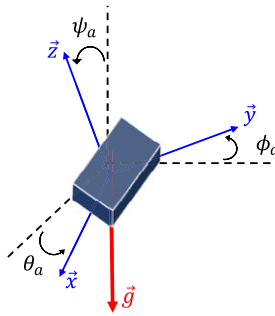


Figure 2. Schematic illustration of the accelerometer-derived inclination angles.

By aligning the IMU sensor frame with the Earth’s reference frame, the algorithm computes the accelerometer’s orientation angles (ϕ_a, θ_a, ψ_a , illustrated in Figure 2) relative to the Earth’s axes:

- ϕ_a (roll): Rotation about the Earth’s X-axis.
- θ_a (pitch): Rotation about the Earth’s Y-axis.
- ψ_a : Angle between the IMU’s Z-axis and the gravity vector, serving as yaw approximation.

These angles (Eqs. 2.6–2.8) are derived from transformed accelerometer measurements $\tilde{\mathbf{a}}_{\text{ref}} = (\tilde{a}_{\text{ref},x}, \tilde{a}_{\text{ref},y}, \tilde{a}_{\text{ref},z})$ (Fisher, 2010; Pedley, 2013). In upper limb motion analysis, this yaw approximation is particularly effective in biomechanically constrained scenarios due to anatomical coupling. Movements such as shoulder elevation or forearm rotation inherently alter the IMU’s inclination relative to gravity, correlating with task-specific orientation changes.

$$\phi_a = \arctan 2 \left(\frac{\tilde{a}_{\text{ref},y}}{\sqrt{\tilde{a}_{\text{ref},x}^2 + \tilde{a}_{\text{ref},z}^2}} \right) \tag{2.6}$$

$$\theta_a = \arctan 2 \left(\frac{\tilde{a}_{\text{ref},x}}{\sqrt{\tilde{a}_{\text{ref},y}^2 + \tilde{a}_{\text{ref},z}^2}} \right) \tag{2.7}$$

$$\psi_a = \arctan 2 \left(\frac{\sqrt{\tilde{a}_{\text{ref},x}^2 + \tilde{a}_{\text{ref},y}^2}}{\tilde{a}_{\text{ref},z}} \right) \tag{2.8}$$

Following this, an update step refines estimates using gyroscope data, as described in Equations (2.9) and (2.10). Here, \mathbf{H}_ω maps the state vector to gyroscope measurements, and \mathbf{R}_ω characterizes gyroscope noise.

$$\mathbf{K}_\omega = \mathbf{P}_{k|k-1} \cdot \mathbf{H}_\omega^T \cdot (\mathbf{H}_\omega \cdot \mathbf{P}_{k|k-1} \cdot \mathbf{H}_\omega^T + \mathbf{R}_\omega)^{-1} \tag{2.9}$$

$$\mathbf{x}_{k|k} = \mathbf{x}_{k|k-1} + \mathbf{K}_\omega \cdot (\omega_k - \mathbf{H}_\omega \cdot \mathbf{x}_{k|k-1}) \tag{2.10}$$

Finally, the accelerometer-derived angles correct the state estimate via Equations (2.11) and (2.12). Here, \mathbf{H}_a maps the state vector to accelerometer measurements, and \mathbf{R}_a characterizes accelerometer noise. By fusing accelerometer-derived angles with gyroscope data, the algorithm corrects gyroscope drift across all three axes.

$$\mathbf{K}_a = \mathbf{P}_{k|k} \cdot \mathbf{H}_a^T \cdot (\mathbf{H}_a \cdot \mathbf{P}_{k|k} \cdot \mathbf{H}_a^T + \mathbf{R}_a)^{-1} \tag{2.11}$$

$$\mathbf{x}_{k+1|k} = \mathbf{x}_{k|k} + \mathbf{K}_a \cdot \left(\begin{bmatrix} \phi_a \\ \theta_a \\ \psi_a \end{bmatrix} - \mathbf{H}_a \cdot \mathbf{x}_{k|k} \right) \tag{2.12}$$

The Kalman gain matrices (\mathbf{K}_ω and \mathbf{K}_a) weight the contributions of gyroscope and accelerometer data, ensuring optimal fusion of sensor inputs.

2.2. Upper limb kinematics estimation from IMU data

To transform the orientation data from IMU sensors into joint angles, this study models the kinematics of the upper extremity, focusing on the shoulder, elbow, and wrist joints, as illustrated in Figure 3.

Initially, the IMU sensors are aligned with the Earth frame. This alignment ensures that the sensor frames are consistent with the anatomical frames. The relative quaternion, $\mathbf{q}_{\text{relative}}$, between two consecutive segments represents joint variations due to movement, as shown in Equation (2.13). Here, \mathbf{q}_1 and \mathbf{q}_2 represent the orientations of the first and second segments, respectively.

$$\mathbf{q}_{\text{relative}} = \mathbf{q}_1^{-1} \cdot \mathbf{q}_2 \tag{2.13}$$

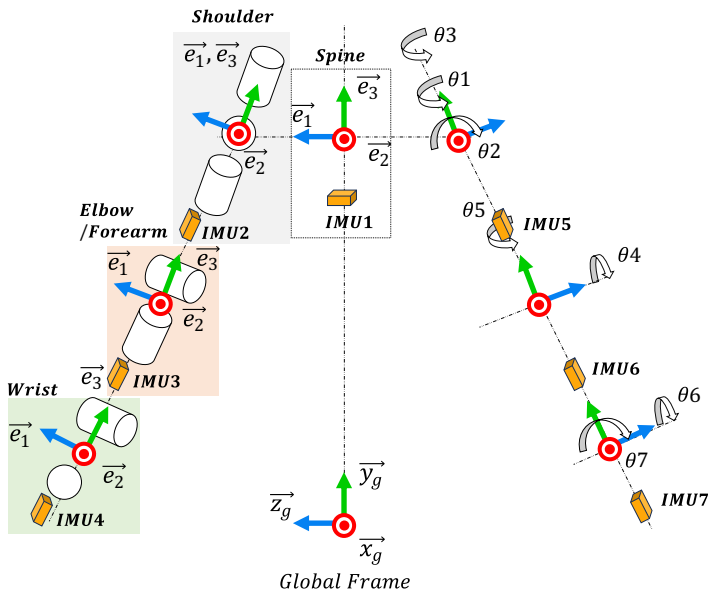


Figure 3. Representation of upper body kinematics, including the spine and upper limbs.

The joint angles are defined as rotations around the X, Y, and Z axes. Depending on the rotation sequence, joint angles θ_x , θ_y , and θ_z are estimated from the quaternions. For each joint, quaternions are calculated based on their respective Euler sequences:

- For the shoulder joint, $\mathbf{q}_{\text{shoulder}}$ is computed using the Y-X-Z rotation order, considering the thorax and upper arm segments.
- For the elbow joint, $\mathbf{q}_{\text{elbow}}$ is computed using the X-Z-Y rotation order, considering the upper arm and forearm segments.
- For the wrist joint, $\mathbf{q}_{\text{wrist}}$ is computed using the X-Y-Z rotation order, considering the forearm and hand segments.

These computations assume the shoulder is initially abducted 90° in the frontal plane and the forearm is fully pronated.

Given $\mathbf{q}_{\text{relative}} = [q_w, q_x, q_y, q_z]$, the joint angles are calculated as shown in Equations (2.14)–(2.16). Here, θ_1 represents flexion/extension, θ_2 represents abduction/adduction, and θ_3 represents internal/external rotation of the shoulder joint.

$$\theta_1 = \arcsin(2(q_w q_x - q_y q_z)) \quad (2.14)$$

$$\theta_2 = \arctan 2\left(2(q_x q_z - q_w q_y), (q_w^2 - q_x^2 - q_y^2 + q_z^2)\right) \quad (2.15)$$

$$\theta_3 = \arctan 2\left(2(q_x q_y + q_w q_z), (q_w^2 - q_x^2 + q_y^2 - q_z^2)\right) \quad (2.16)$$

For the elbow joint, the joint angles are calculated as shown in Equations (2.17)–(2.18). Here, θ_4 represents flexion/extension, and θ_5 represents pronation-supination rotation.

$$\theta_4 = \arctan 2\left(2(q_w q_x + q_y q_z), (q_w^2 - q_x^2 + q_y^2 - q_z^2)\right) \quad (2.17)$$

$$\theta_5 = \arctan 2\left(2(q_w q_y + q_x q_z), (q_w^2 + q_x^2 - q_y^2 - q_z^2)\right) \quad (2.18)$$

For the wrist joint, the joint angles are calculated as shown in Equations (2.19)–(2.20). Here, θ_6 represents flexion/extension, and θ_7 represents adduction/abduction.

$$\theta_6 = \arctan 2\left(-2(q_y q_z - q_w q_x), \left(1 - 2(q_x^2 + q_y^2)\right)\right) \quad (2.19)$$

$$\theta_7 = \arctan 2\left(-2(q_x q_y - q_w q_z), \left(1 - 2(q_y^2 + q_z^2)\right)\right) \quad (2.20)$$

2.3. Experimental setup for the evaluation of the proposed method

The evaluation of the proposed algorithm for sensor orientation estimation is conducted in two distinct phases. In Phase 1, the algorithm's performance is assessed against renowned sensor fusion algorithms using controlled robotic movements. In Phase 2, the algorithm is tested in a real-world scenario using a wearable IMU-based system for human motion analysis. The 9-degree of freedom (DoF) MPU-9250

micro-electromechanical systems (MEMS)-based IMU used in this study includes: A 3-axis accelerometer ($\pm 16g$ range), a 3-axis gyroscope ($\pm 2000^\circ/s$ range), and a 3-axis magnetometer ($\pm 4800 \mu T$ range). This sensor was employed in both the controlled robotic experiments and the human motion analysis trials.

2.3.1. Phase 1: Controlled environment testing

In Phase 1, the 9-DoF IMU is mounted on the end effector of a 5-axis SCORBOT ER-9 PRO robot. The X-, Y-, and Z-axes of the sensor are aligned with those of the robot (**Figure 4**), ensuring that the IMU's orientation accurately reflects the rotational motions of the robot's end effector. The setup, connected to an ARDUINO Mega2560 microcontroller, facilitates the capture of rotation data around the three axes of the sensor. A total of 20 repetitions are performed for each rotational axis to evaluate the algorithm's accuracy.

2.3.2. Phase 2: Human motion analysis

The second phase involves implementing the algorithm in a wearable IMU-based system for upper limb motion capture. The system comprises seven IMU nodes attached to the upper arm, forearm, and hand segments, operating at a sample rate of 10 Hz. Three healthy female volunteers (age: 28 ± 2 years; height: 167 ± 3.5 cm; weight: 65.5 ± 3 kg) participated in the acquisition session. They were equipped with wearable sensors and 28 reflective markers. The 3D trajectories of the markers were collected at 100 Hz using a Vicon Optical Motion Capture (OMC) system with 38 cameras (Vicon, Oxford Metrics Ltd, Oxford, UK).

After a 30-s T-pose for calibration, participants performed 10 repetitions of upper body movements representing the key degrees of freedom. These included: 3 movements at the shoulder: θ_1 (flexion/extension), θ_2 (abduction/adduction), and θ_3 (internal/external rotation); two movements at the elbow: θ_4 (flexion/extension) and θ_5 (pronation/supination); and two movements at the wrist: θ_6 (flexion/extension) and θ_7 (radial/ulnar deviation). The aim was to measure the movements within each DoF individually.

Data from both systems were compared to assess the validity of the IMU-based system against the gold standard OMC system. The data obtained from the OMC system were processed using the Plugin-Gait (PiG) upper body model for kinematic calculations, as illustrated in **Figure 5**.

2.4. Data analysis

2.4.1. Error analysis compared to encoders and filtering techniques

IMU sensor calibration, orientation estimation, and encoder measurement calculations were performed according to the study by Baklouti et al. (2022). Statistical measures were used to compare the IMU

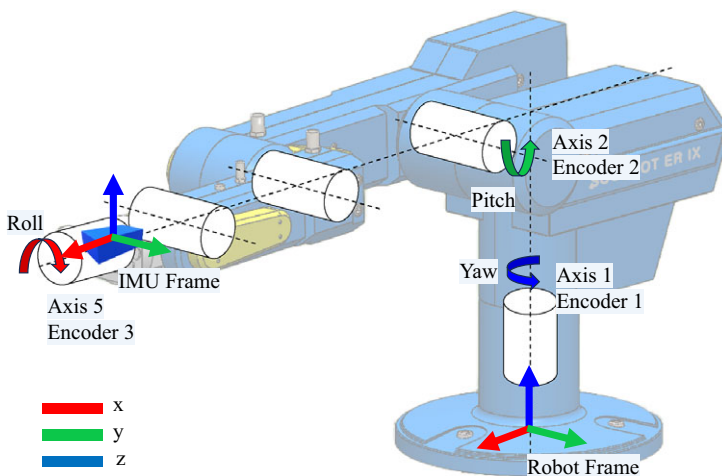


Figure 4. Experimental setup with the MPU-9250 IMU mounted on the SCORBOT ER-9 PRO robot.

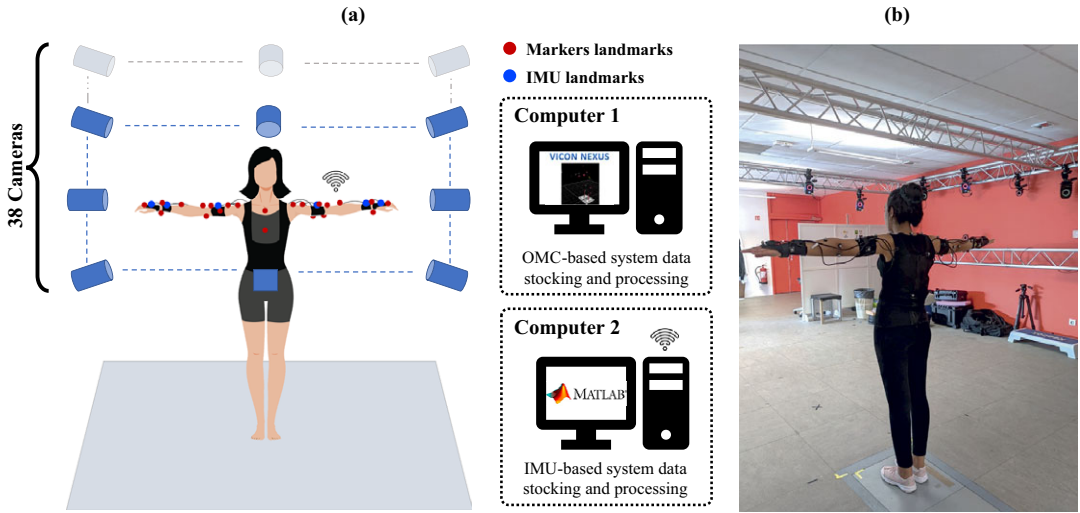


Figure 5. Visual representation of the experimental setup: (a) schematic illustration and (b) real-life experimental setup of IMU-based and OMC-based systems.

system’s performance against the robot’s reference encoder measurements (considered as the ground truth). Additionally, comparisons were made with the DSKF and complementary filter for orientation estimation around the X, Y, and Z-axes.

The DSKF, as described in Sabatelli et al. (2013), employs a two-step correction process for orientation estimation using quaternions. During the first stage, roll and pitch angles are corrected by comparing the expected and measured gravity vectors from the accelerometer. In the second stage, the yaw angle is refined using magnetometer data.

The complementary filter integrates the high-frequency response of gyroscope data with the low-frequency response of accelerometer and magnetometer data. It uses the accelerometer to correct roll and pitch angles and the magnetometer to correct the yaw angle. The filter is formulated as shown in Equation (2.21):

$$\hat{\theta}_t = \alpha \left(\hat{\theta}_{t-1} + \omega_t \Delta t \right) + (1 - \alpha) \theta_{\text{accel/mag},t} \tag{2.21}$$

where $\hat{\theta}_t$ is the estimated orientation at time t , $\hat{\theta}_{t-1}$ is the estimated orientation at the previous time step, ω_t is the angular rate measured by the gyroscope, Δt is the time step, $\theta_{\text{accel/mag},t}$ is the orientation calculated from the accelerometer and magnetometer data, and α is the filter gain, typically chosen to balance the contributions of the gyroscope and accelerometer/magnetometer. In this study, $\alpha = 0.9$.

The metrics utilized included the correlation coefficient (r), which indicates the linear relationship strength and direction between the IMU and encoder measurements; the coefficient of determination (r^2), representing the variance proportion in encoder measurements explained by the IMU data; RMSE, measuring the average magnitude of errors; intra-class correlation coefficient (ICC, two-way mixed effects), assessing the measurement reliability and consistency; lower limit of agreement (LoA), providing the range capturing most differences between IMU and encoder measurements, indicating agreement; mean absolute error (MAE), computing the average absolute differences; and normalized mean bias error (NMBE), reflecting the average bias of the IMU measurements relative to the encoders.

2.4.2. Kinematic analysis using statistical parametric mapping

To assess the agreement between IMU and VICON (considered as the ground truth) measurements, a set of metrics was employed, including RMSE, MAE, NMBE, and r^2 . These metrics were further

contextualized by considering the ROM for each joint, allowing for a more nuanced interpretation of the error measures. To statistically evaluate potential differences between IMU and VICON measurements for each DoF, a curve analysis was performed using statistical parametric mapping (SPM) with a two-tailed paired t-test (Flandin and Friston, 2008). This analysis included a two-tailed paired t-test to compare joint angles from both systems, setting a significance level at $\alpha = 0.05$. Data were synchronized and time normalized within MATLAB after aligning to the first movement peak, formatted into 101 data points (0–100%). The SPM{t} statistic was computed at each time node to determine the level of similarity between the curves. Regions where SPM{t} exceeded the critical t-value, indicating statistically significant differences, were identified and analyzed to pinpoint phases in the movement cycle with notable discrepancies.

3. Results

3.1. Error analysis results

The performance of sensor fusion methods, double-stage Kalman, complementary, and the proposed filters, was evaluated across different orientations: Roll, pitch, and yaw. Figure 6 shows a sample of the experiment result. The results are summarized in Table 1.

All methods demonstrated very high correlation coefficients ($R > 0.997$) and coefficients of determination ($r^2 > 0.995$) across all orientations, indicating strong linear relationships and predictive accuracy with the reference data. However, our proposed magnetometer-free method outperformed the other methods in terms of RMSE and MAE, especially in the yaw orientation. This suggests that, in a controlled environment, it provides better accuracy in estimating true values. Additionally, the proposed method exhibited the lowest NMBE across all orientations, indicating less measurement bias relative to the reference. The LoA analysis also highlighted the superior performance of the proposed method. It showed narrower ranges between the lower and upper LoAs, particularly in the yaw orientation, which suggests better agreement with the reference measurements.

3.2. Validity study results

Figures 7–9 summarize the results of the data analysis phase comparing IMU-derived measurements to the VICON PiG model. All IMU traces presented in these figures were processed using the proposed approach. The std metrics reported in these figures reflect the variability between subjects and repetitions during the experimental trials. Specifically, it quantifies the differences in joint angle measurements across the volunteers performing ten repetitions of upper limb movements. In the figures, the notation t^* refers to the critical t-value, which identifies statistically significant differences between the IMU-based and reference VICON systems.

The RMSE across all joints varied from 5.352° for wrist adduction-abduction to 12.075° for elbow pronation-supination. The MAE ranged from 3.688° for wrist adduction-abduction to 7.501° for elbow flexion-extension. The NMBE showed a minimal value of -0.839 in wrist flexion-extension, indicating potential underestimation, to a maximum of 0.143 in elbow flexion-extension, suggesting slight overestimation. These error metrics fall within 3–12.4% of the ROM (Namdari et al., 2012; Raiss et al., 2007) of the studied joints. The r^2 values, reflecting the correlation between the IMU and VICON data, were strongly positive, ranging from 0.890 in wrist adduction-abduction to 0.974 in shoulder flexion-extension.

In shoulder joint motion monitoring, the comparative evaluation of IMU- and OMC-based systems across various DoF using SPM analysis is depicted in Figure 7. The analysis shows no significant differences in shoulder DoF θ_1 , θ_2 , and θ_3 between the IMU-based and the reference Vicon OMC system across all trials. In elbow joint motion monitoring, Figure 8 shows that there were no significant differences observed in elbow θ_4 DoF during flexion-extension trials. However, significant differences were found in forearm θ_5 DoF during pronation-supination trials between 44 and 59% of the motion

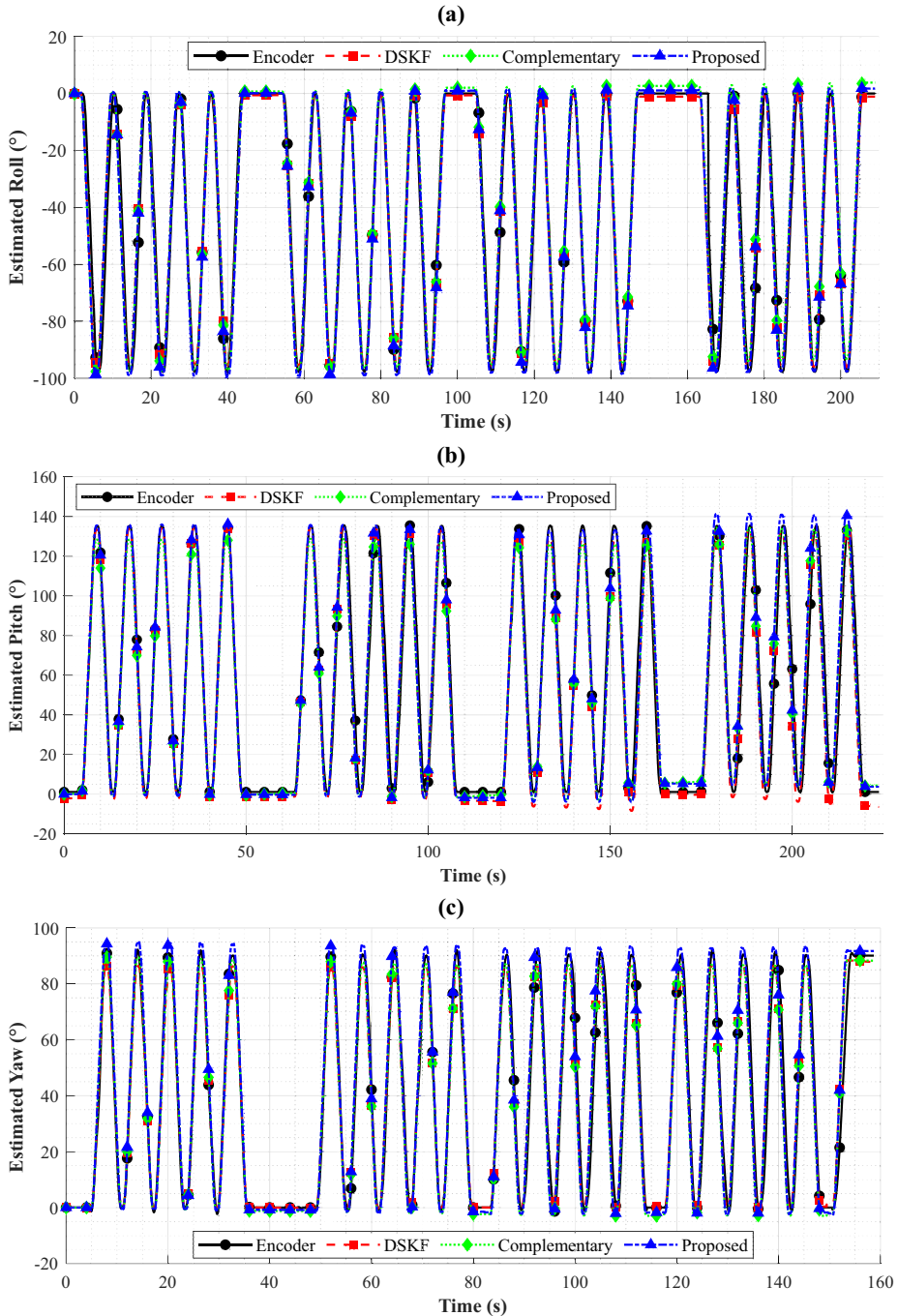


Figure 6. Sample results of orientation estimation for (a) Roll, (b) Pitch, and (c) Yaw trials on a SCORBOT ER-9 Pro robot, comparing the estimates of a double-stage Kalman filter, a complementary filter, and our proposed approach against the robot's encoder reference measurements.

cycles. For the wrist joint motion monitoring, Figure 9 shows that significant differences in θ_6 DoF were observed between 15 and 33% during flexion-extension, and θ_7 DoF between 5 and 6.5% and 44 and 57% during adduction-abduction motion cycles.

Table 1. Error analysis of sensor fusion methods: double-stage Kalman, complementary, and proposed filters Across roll, pitch, and yaw orientations

	Metric	Kalman	Complementary	Proposed
Roll	R (\pm std)	0.9992 (\pm 0.0003)	0.9993 (\pm 0.0003)	0.9992 (\pm 0.0003)
	r^2 (\pm std)	0.9985 (\pm 0.0006)	0.9985 (\pm 0.0006)	0.9985 (\pm 0.0006)
	RMSE (deg \pm std)	2.049 (\pm 0.262)	2.954 (\pm 0.324)	1.639 (\pm 0.275)
	MAE (deg \pm std)	1.657 (\pm 0.226)	2.460 (\pm 0.300)	1.317 (\pm 0.218)
	NMBE (\pm std)	0.0276 (\pm 0.0043)	0.0503 (\pm 0.0081)	0.0202 (\pm 0.0054)
	Lower LoA (deg \pm std)	-4.414 (\pm 0.579)	-5.870 (\pm 0.574)	-3.549 (\pm 0.609)
	Upper LoA (deg \pm std)	1.845 (\pm 0.418)	1.203 (\pm 0.496)	1.672 (\pm 0.546)
Pitch	R (\pm std)	0.9976 (\pm 0.0009)	0.9977 (\pm 0.0009)	0.9977 (\pm 0.0009)
	r^2 (\pm std)	0.9953 (\pm 0.0018)	0.9953 (\pm 0.0018)	0.9953 (\pm 0.0017)
	RMSE (deg \pm std)	3.407 (\pm 0.716)	3.471 (\pm 0.660)	3.076 (\pm 0.594)
	MAE (deg \pm std)	2.803 (\pm 0.604)	2.873 (\pm 0.600)	2.554 (\pm 0.525)
	NMBE (\pm std)	0.0418 (\pm 0.0223)	0.0414 (\pm 0.0192)	0.0312 (\pm 0.0198)
	Lower LoA (deg \pm std)	-3.485 (\pm 1.031)	-3.742 (\pm 0.957)	-3.764 (\pm 1.009)
	Upper LoA (deg \pm std)	7.245 (\pm 1.519)	7.462 (\pm 1.424)	6.577 (\pm 1.367)
Yaw	R (\pm std)	0.9986 (\pm 0.0013)	0.9986 (\pm 0.0014)	0.9986 (\pm 0.0015)
	r^2 (\pm std)	0.9972 (\pm 0.0027)	0.9972 (\pm 0.0027)	0.9971 (\pm 0.0030)
	RMSE (deg \pm std)	2.998 (\pm 0.667)	3.042 (\pm 0.613)	2.447 (\pm 0.680)
	MAE (deg \pm std)	2.491 (\pm 0.516)	2.473 (\pm 0.496)	2.006 (\pm 0.566)
	NMBE (\pm std)	0.0522 (\pm 0.0093)	0.0504 (\pm 0.0081)	0.0370 (\pm 0.0054)
	Lower LoA (deg \pm std)	-1.357 (\pm 0.913)	-1.764 (\pm 0.933)	-1.875 (\pm 1.190)
	Upper LoA (deg \pm std)	6.006 (\pm 1.548)	6.248 (\pm 1.431)	5.164 (\pm 1.616)

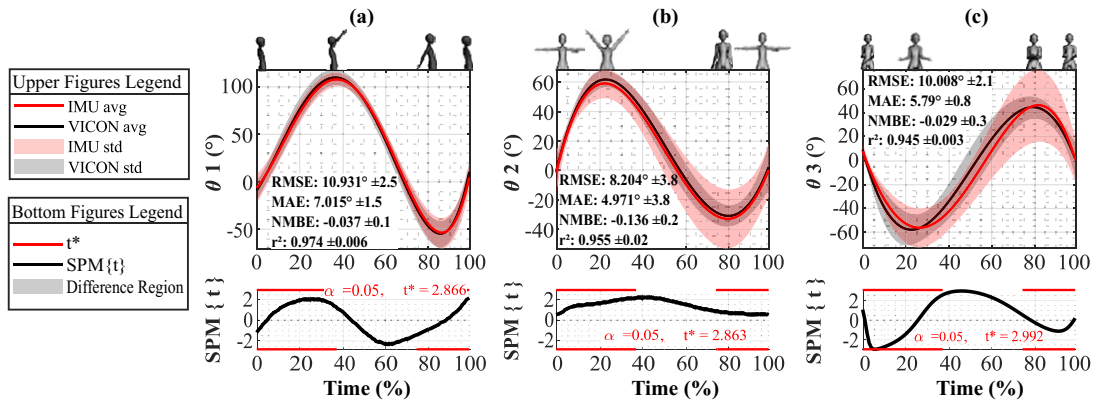


Figure 7. Comparative evaluation of IMU- and OMC-based systems for (a) shoulder flexion-extension θ_1 , (b) shoulder adduction-abduction θ_2 , and (c) shoulder internal-external rotation θ_3 DoF with SPM Analysis.

4. Discussion

In this study, we proposed a novel magnetometer-free approach integrating the refined KF to correct orientation estimation. This approach aligns with clinical biomechanical practices prioritizing relative segment angles (e.g., arm elevation) over absolute heading (Cutti et al., 2007). While pure yaw about the global vertical axis remains unobservable without magnetometers, studies confirm inclination-based metrics quantify functional ranges (e.g., shoulder abduction) with errors 5° (Picerno et al., 2008). The method’s trade-off between sensor limitations and anatomical realities has been validated in applications ranging from stroke rehabilitation to athletic training, demonstrating its effectiveness for upper limb motions characterized by inclination-linked coupled kinematics rather than isolated yaw (Zhou et al., 2006).

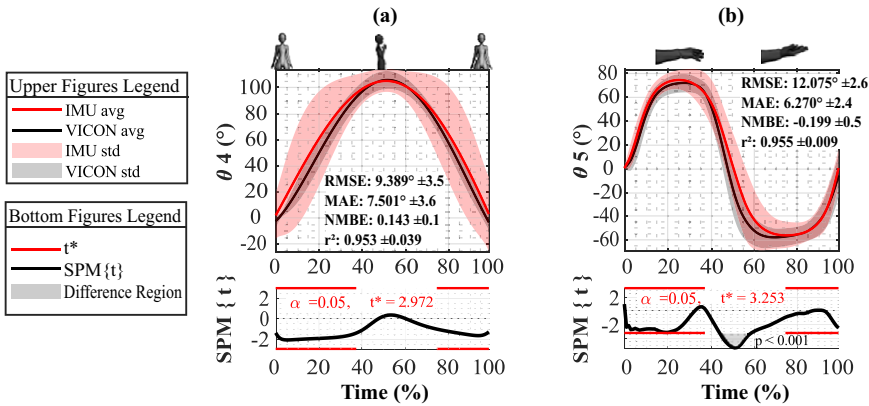


Figure 8. Comparative evaluation of IMU- and OMC-based systems for (a) elbow flexion-extension θ_4 , and (b) forearm pronation-supination θ_5 DoF with SPM Analysis.

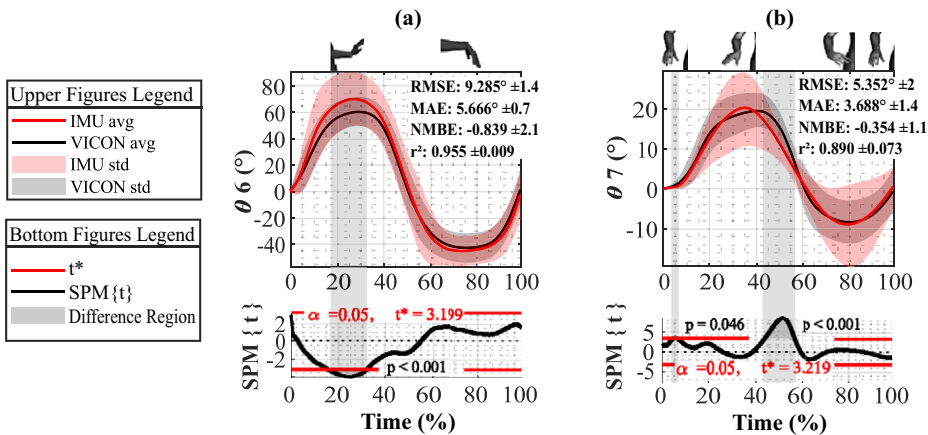


Figure 9. Comparative evaluation of IMU- and OMC-based systems for (a) wrist flexion-extension θ_6 , and (b) wrist adduction-abduction θ_7 DoF with SPM Analysis.

While extended Kalman filter (EKF) algorithms are typically preferred for human motion estimation due to their ability to handle nonlinear dynamics (Sabatini, 2011), our approach employs a standard KF through careful system design. Nonlinear accelerometer-derived orientation angles (ϕ_a, θ_a, ψ_a) are pre-computed and treated as direct linear measurements within the filter, eliminating the need for EKF-based Jacobian linearization. The measurement matrix \mathbf{H} directly maps the state vector (containing orientation angles and gyroscope biases) to these preprocessed measurements, as validated in lightweight inertial fusion frameworks (Valenti et al., 2016). The gyroscope-driven prediction step utilizes a first-order kinematic model, which is valid for small Δt by avoiding nonlinear error growth (Luinge and Veltink, 2005). This design reduces computational complexity to $\mathcal{O}(n^3)$ compared to EKF's $\mathcal{O}(n^3)$ plus Jacobian calculations, a critical advantage for real-time wearable IMU systems with limited processing resources (Särkkä, 2013). By decoupling nonlinear operations from the filtering process and including linearized state transitions, our approach ensures sensor orientation estimation while prioritizing computational efficiency.

In controlled robotic movements, the proposed magnetometer-free orientation estimation approach showed a superior performance, particularly in yaw estimation. This can be attributed to its combination of gyroscope and accelerometer data fusion within a KF framework, along with its direct alignment of the

sensor frame with the global frame using accelerometer-derived angles. The proposed method includes the strengths of the gyroscope at capturing short-term dynamic changes in orientation and accelerometer at capturing long-term dynamic changes in orientation (Chen and Rong, 2023; Trinh et al., 2020). By fusing these measurements, the algorithm compensates for the inherent limitations of each sensor, such as drift in gyroscope readings and noise in accelerometer data.

The traditional methods, however, rely on magnetometers for yaw correction, making them susceptible to magnetic disturbances (Chen and Rong, 2023). The proposed method's independence from magnetometer data contribute to more accurate yaw estimates, as evidenced by the lower RMSE, MAE, and NMBE values. This robustness against disturbances makes it suitable for diverse environments, including industrial applications. In addition, in real environments such as human motion, the variability in error metrics for the joints, observed across different movements, was noted to be within 3–12.4% of the joints' ROM. This variability falls within acceptable limits for various motion capture technologies (Morrow et al., 2017; Schiefer et al., 2014; Song et al., 2023), though it is unsuitable for applications requiring high precision (Berner et al., 2020; Nakano et al., 2020). Additionally, the r^2 values ranged from 0.890 to 0.974, indicating a strong positive correlation and highlighting a high degree of correlation between IMU and VICON data.

The variability in IMU-based system measurements is further demonstrated by the SPM analysis where motion cycle intervals with significant differences are identified. Namely, a significant difference was identified between IMU-based and OMC for the elbow joints motion cycles between 44 and 59% in θ_5 of the cycles of forearm pronation-supination, corresponding to the return to the neutral position in the pronation phase.

Similarly, a significant difference between the two technologies was identified for the wrist joint. This difference is specifically in the wrist joints between 15 and 33% of wrist flexion-extension cycle θ_6 , corresponding to the maximal flexion.

A significant difference was also identified for the wrist joint in θ_7 , where the IMU-based system underestimated the joint angle value between 5 and 6.5% of the motion cycle, corresponding to the beginning of the abduction phase, and between 44 and 57% of the motion cycle, corresponding to the end of the abduction phase. This could be related to the inherent nature of IMU as a similar observation has been done by Mittag et al., 2020, who reported that IMU may not always capture the full range of wrist abduction, suggesting underestimation in some cases.

The variations observed among subjects in the precision of the joint measurements using the IMU-based system may be attributed to intersubject variations in sensor placement and movement-induced artifacts stemming from the sensor attachment methodology, as previously established in the literature (Wang et al., 2022).

Furthermore, it is noteworthy to mention that the precision of measurements obtained using IMU technology may decrease as the movement speed increases (Cooper et al., 2009). It is important to note that variations between the joint angles obtained using IMU-based and OMC technology are an inherent result of the different definitions of the segment axes and the distinct effects of soft tissue artifacts on the measurements (Cutti et al., 2007).

While OMC systems have been established to provide reliable ground truth, it is important to acknowledge that, like all noninvasive techniques, OMC systems are subject to soft tissue artifact effects. According to Morrow et al. (2011), the precision of a standard OMC system is within 3° of angular accuracy for human kinematics.

5. Conclusion

This study has addressed the critical challenges in sensor fusion for wearable IMU by proposing a magnetometer-free KF approach for robust and accurate orientation estimation. Traditional IMU-based systems, which often rely on magnetometers, face significant limitations due to magnetic interference and the need for extensive calibration processes. By eliminating the dependency on magnetometers, our approach enhances the versatility and reliability of IMU systems in diverse environments.

The proposed method effectively integrates gyroscope and accelerometer data using a refined KF, aligning the sensor frame with the Earth's frame. This approach demonstrated superior performance across multiple metrics. In controlled robotic movements, the novel algorithm achieved an RMSE of 2.447° and MAE of 2.006° for yaw orientation, outperforming established techniques. The proposed method also showed the lowest NMBE across all orientations, indicating minimal measurement bias relative to reference data. The LoA analysis confirmed the results of the proposed method, with narrower ranges between the lower and upper LoAs, especially in yaw orientation, suggesting better agreement with reference measurements.

In real-world applications, such as upper limb motion monitoring, the variability in error metrics for joint measurements was within 3–12.4% of the joints' ROM. This variability is acceptable for many motion capture technologies, although further refinement is needed for high-precision applications. The method demonstrated low error metrics and a strong positive correlation with VICON data, highlighting the high degree of agreement between the IMU-based and the OMC systems.

The SPM analysis further revealed motion cycle intervals with significant differences between the IMU-based system and the OMC system. Short but significant intervals of differences in joint motion cycles were observed in the elbows and wrists. These discrepancies are likely related to the inherent nature of IMU, as they sometimes underestimate or overestimate joint angles, particularly in complex movements.

The proposed magnetometer-free KF approach offers a promising alternative for accurate and reliable orientation estimation in environments with magnetic distortions. By minimizing manual calibration requirements and incorporating detailed algorithmic refinements, this method has significant potential for improving sensor fusion technology in dynamic and complex settings. Future research will focus on optimizing the algorithm for real-time applications on devices with limited processing power and enhancing the method's accuracy and stability for diverse motion dynamics.

Data availability statement. The datasets collected and analyzed during this study are not publicly available due to confidentiality and ethical restrictions related to human participant data.

Authorship contribution. Conceptualization: S.B. (Souha Baklouti), T.R., and A.C.; Data collection: S.B. (Souha Baklouti); Data curation: S.B. (Souha Baklouti); Formal analysis: S.B. (Souha Baklouti); Funding acquisition: A.S.; Investigation: S.B. (Souha Baklouti) and T.R.; Methodology: S.B. (Souha Baklouti), S.B. (Sami Bennour), T.R., and A.C.; Project administration: S.B. (Sami Bennour) and A.S.; Resources: A.S.; Software development: S.B. (Souha Baklouti); Supervision: S.B. (Sami Bennour) and A.S.; Validation: S.B. (Souha Baklouti), S.B. (Sami Bennour), T.R., and A.C.; Writing—original draft preparation: S.B. (Souha Baklouti); Writing—review and editing: T.R., A.C., S.B. (Sami Bennour), and A.S. All authors have read and agreed to the published version of the manuscript. All authors approved the final submitted draft.

Funding statement. This project is carried out under the MOBIDOC scheme, funded by The Ministry of Higher Education and Scientific Research through the PromEsSE project and managed by the ANPR (The National Agency for the advancement of scientific research).

Competing interests. The authors declare no competing interests exist.

Ethical standard. The study was conducted in accordance with the Declaration of Helsinki and approved by the Ethics Committee for Life and Health Sciences Research of the Higher Institute of Biotechnology of Monastir (ISBM) (protocol code CERSVS/ISBM 018/2023).

References

- Baklouti S, Chaker A, Rezgui T, Sahbani A, Bennour S and Laribi MA** (2024) A novel IMU-based system for work-related musculoskeletal disorders risk assessment. *Sensors* **24**(11), 3419. <https://doi.org/10.3390/s24113419>
- Baklouti S, Rezgui T, Chaouch A, Chaker A, Mefteh S, Sahbani A and Bennour S** (2022) IMU based serial manipulator joint angle monitoring: Comparison of complementary and double stage Kalman filter data fusion. In Walha, Lassaadand, Jarraya, Abdessalemand, Djemal, Fathiand, Chouchane, Mnaouarand, Aifaoui, Nizarand, Chaari, Fakherand, Abdennadher, Moezand, Benamara, Abdelmajidand, Haddar, Mohamed *Design and Modeling of Mechanical Systems - V*. Cham: Springer International Publishing, pp. 215–224. https://doi.org/10.1007/978-3-031-14615-2_25
- Bernal-Polo P and Martínez Barberá H** (2017) Orientation estimation by means of extended Kalman filter, quaternions, and charts. *Journal of Physical Agents (JoPha)* **8**(1), 11–24. <https://doi.org/10.14198/jopha.2017.8.1.03>

- Berner K, Cockcroft J and Louw Q** (2020) Kinematics and temporospatial parameters during gait from inertial motion capture in adults with and without HIV: A validity and reliability study. *Biomedical Engineering Online* **19**(1), 1–25. <https://doi.org/10.1186/s12938-020-00802-2>
- Chen Y and Rong H** (2023) A customized extended Kalman filter for removing the impact of the magnetometer's measurements on inclination determination. *Sensors* **23**(24), 9756. <https://doi.org/10.3390/s23249756>
- Cooper G, Sheret I, McMillian L, Siliverdis K, Sha N, Hodgins D, Kenney L and Howard D** (2009) Inertial sensor-based knee flexion/extension angle estimation. *Journal of Biomechanics* **42**(16), 2678–2685. <https://doi.org/10.1016/j.jbiomech.2009.08.004>
- Cutti AG, Giovanardi A, Rocchi L, Davalli A and Sacchetti R** (2007) Ambulatory measurement of shoulder and elbow kinematics through inertial and magnetic sensors. *Medical & Biological Engineering & Computing* **46**(2), 169–178. <https://doi.org/10.1007/s11517-007-0296-5>
- Fain A, McCarthy A, Nindl BC, Fuller JT, Wills JA and Doyle TLA** (2024) IMUs can estimate hip and knee range of motion during walking tasks but are not sensitive to changes in load or grade. *Sensors* **24**(5), 1675. <https://doi.org/10.3390/s24051675>
- Fan B, Li Q and Liu T** (2017) How magnetic disturbance influences the attitude and heading in magnetic and inertial sensor-based orientation estimation. *Sensors* **18**(1), 1–27. <https://doi.org/10.3390/s18010076>
- Fisher CJ** (2010) Using an Accelerometer for Inclination Sensing (Application Note No. AN-1057). Analog Devices. <https://www.analog.com/media/en/technical-documentation/app-notes/an-1057.pdf>
- Flandin G and Friston K** (2008) Statistical parametric mapping (spm). *Scholarpedia* **3**(4), 6232. <https://doi.org/10.4249/scholarpedia.6232>
- Halitim AM, Bouhedda M, Tchoketch-Kebir S and Rebouh S** (2023) Artificial neural network for tilt compensation in yaw estimation. *Transactions of the Institute of Measurement and Control*. <https://doi.org/10.1177/01423312231214832>
- Kim A and Golnaraghi M** (2004) A quaternion-based orientation estimation algorithm using an inertial measurement unit, *PLANS 2004. Position Location and Navigation Symposium* (IEEE Cat. No. 04CH37556) 268–272. <https://doi.org/10.1109/PLANS.2004.1309003>
- Laidig D and Seel T** (2023) VQF: Highly accurate IMU orientation estimation with bias estimation and magnetic disturbance rejection. *Information Fusion* **91**, 187–204. <https://doi.org/10.1016/j.inffus.2022.10.014>
- Luczak S, Zams M, Dąbrowski B and Kuznierewicz Z** (2022) Tilt sensor with recalibration feature based on mems accelerometer. *Sensors* **22**(4), 1504. <https://doi.org/10.3390/s22041504>
- Luinge HJ and Veltink PH** (2005) Measuring orientation of human body segments using miniature gyroscopes and accelerometers. *Medical & Biological Engineering & Computing* **43**(2), 273–282. <https://doi.org/10.1007/bf02345966>
- Madgwick SOH, Harrison AJL and Vaidyanathan R** (2011) Estimation of IMU and MARG orientation using a gradient descent algorithm. *2011 IEEE International Conference on Rehabilitation Robotics*. <https://doi.org/10.1109/icorr.2011.5975346>
- Mittag C, Leiss R, Lorenz K and Seel T** (2020) Development of a home-based wrist range-of-motion training system for children with cerebral palsy. *Automatisierungstechnik* **68**(11), 967–977. <https://doi.org/10.1515/auto-2020-0085>
- Morrow MM, Kaufman KR and An K-N** (2011) Scapula kinematics and associated impingement risk in manual wheelchair users during propulsion and a weight relief lift. *Clinical biomechanics* **26**(4), 352–357. <https://doi.org/10.1016/j.clinbiomech.2010.12.001>
- Morrow MM, Lowndes B, Fortune E, Kaufman KR and Hallbeck MS** (2017) Validation of inertial measurement units for upper body kinematics. *Journal of Applied Biomechanics* **33**(3), 227–232. <https://doi.org/10.1123/jab.2016-0120>
- Nakano N, Sakura T, Ueda K, Omura L, Kimura A, Iino Y, Fukashiro S and Yoshioka S** (2020) Evaluation of 3D markerless motion capture accuracy using openpose with multiple video cameras. *Frontiers in Sports and Active Living* **2**, 1–9. <https://doi.org/10.3389/fspor.2020.00050>
- Namdari S, Yagnik G, Ebaugh DD, Nagda S, Ramsey ML, Williams GR and Mehta S** (2012) Defining functional shoulder range of motion for activities of daily living. *Journal of Shoulder and Elbow Surgery* **21**(9), 1177–1183. <https://doi.org/10.1016/j.jse.2011.07.032>
- Pedley M** (2013) Tilt Sensing Using a Three-Axis Accelerometer (Application Note No. AN3461). NXP Semiconductors. <https://www.nxp.com/docs/en/application-note/AN3461.pdf>
- Picerno P, Cereatti A and Cappaiozzo A** (2008) Joint kinematics estimate using wearable inertial and magnetic sensing modules. *Gait & Posture* **28**(4), 588–595. <https://doi.org/10.1016/j.gaitpost.2008.04.003>
- Raiss P, Rettig O, Wolf S, Loew M and Kasten P** (2007) Das bewegungsausmaß der schulter und des ellenbogens bei alltagsbewegungen in der 3d-bewegungsanalyse. *Zeitschrift für Orthopädie und Unfallchirurgie* **145**(04), 493–498. <https://doi.org/10.1055/s-2007-965468>
- Rogers J, Costello M, Harkins T and Hamaoui M** (2011) Effective use of magnetometer feedback for smart projectile applications. *Navigation* **58**(3), 203–219. <https://doi.org/10.1002/j.2161-4296.2011.tb02581.x>
- Sabatelli S, Galgani M, Fanucci L and Rocchi A** (2013) A double-stage Kalman filter for orientation tracking with an integrated processor in 9-D IMU. *IEEE Transactions on Instrumentation and Measurement* **62**(3), 590–598. <https://doi.org/10.1109/tim.2012.2218692>
- Sabatini AM** (2011) Kalman-filter-based orientation determination using inertial/magnetic sensors: Observability analysis and performance evaluation. *Sensors* **11**(10), 9182–9206. <https://doi.org/10.3390/s111009182>
- Särkkä S** (2013) *Bayesian Filtering and Smoothing*. New York, USA: Cambridge University Press.
- Schiefer C, Ellegast RP, Hermanns I, Kraus T, Ochsmann E, Larue C and Plamondon A** (2014) Optimization of inertial sensor-based motion capturing for magnetically distorted field applications. *Journal of Biomechanical Engineering* **136**(12), 121008-1–121008-8. <https://doi.org/10.1115/1.4028822>

- Song K, Hullfish TJ, Silva RS, Silbernagel KG and Baxter JR** (2023) Markerless motion capture estimates of lower extremity kinematics and kinetics are comparable to marker-based across 8 movements. *Journal of Biomechanics* **157**, 111751. <https://doi.org/10.1101/2023.02.21.526496>
- Trinh X-D, Le M-C and Tran N-H** (2020) IMU calibration methods and orientation estimation using extended Kalman filters. In Cortes, Tobar, Dario, Fernando and Hoang, Duy, Voand Trong, Dao, Tran *Aeta 2019: Recent Advances in Electrical Engineering and Related Sciences: Theory and Application*. Cham: Springer International Publishing, pp. 541–551. https://doi.org/10.1007/978-3-030-53021-1_55
- Valenti RG, Dryanovski I and Xiao J** (2016) A linear Kalman filter for MARG orientation estimation using the algebraic quaternion algorithm. *IEEE Transactions on Instrumentation and Measurement* **65**(2), 467–481. <https://doi.org/10.1109/tim.2015.2498998>
- Vigne M, Khoury AE, Meglio FD and Petit N** (2020) State estimation for a legged robot with multiple flexibilities using IMUs: A kinematic approach. *IEEE Robotics and Automation Letters* **5**(1), 195–202. <https://doi.org/10.1109/lra.2019.2953006>
- Wang SL, Civillico G, Niswander W and Kontson KL** (2022) Comparison of motion analysis systems in tracking upper body movement of myoelectric bypass prosthesis users. *Sensors* **22**(8), 2953. <https://doi.org/10.3390/s22082953>
- Xiaoping Y, Bachmann E and McGhee R** (2008) A simplified quaternion-based algorithm for orientation estimation from earth gravity and magnetic field measurements. *IEEE Transactions on Instrumentation and Measurement* **57**(3), 638–650. <https://doi.org/10.1109/tim.2007.911646>
- Yadav N and Bleakley C** (2014) Accurate orientation estimation using AHRS under conditions of magnetic distortion. *Sensors* **14**(11), 20008–20024. <https://doi.org/10.3390/s141120008>
- Zhou H, Hu H and Tao Y** (2006) Inertial measurements of upper limb motion. *Medical & Biological Engineering & Computing* **44**(6), 479–487. <https://doi.org/10.1007/s11517-006-0063-z>
- Zihajehzadeh S and Park EJ** (2017) A novel biomechanical model-aided IMU/UWB fusion for magnetometer-free lower body motion capture. *IEEE Transactions on Systems, Man, and Cybernetics: Systems* **47**(6), 927–938. <https://doi.org/10.1109/tsmc.2016.2521823>

Cite this article: Baklouti S, Rezgui T, Chaker A, Sahbani A and Bennour S (2025) Novel magnetometer-free inertial-measurement-unit-based orientation estimation approach for measuring upper limb kinematics. *Wearable Technologies*, 6, e28. doi:<https://doi.org/10.1017/wtc.2025.10003>